WWZ, ZZZ, and $WW\gamma$ production at e^+e^- colliders

V. Barger and T. Han
Physics Department, University of Wisconsin, Madison, Wisconsin 53706

R. J. N. Phillips
Rutherford Appleton Laboratory, Chilton, Didcot, Oxon, England
(Received 19 August 1988)

We discuss the prospects for the detection of WWZ, ZZZ, and $WW\gamma$ events at a future e^+e^- supercollider with c.m. energy 0.35–2.0 TeV. These modes provide tests of triple and quartic gauge-boson couplings. WWZ and ZZZ modes also provide tests of a neutral Higgs boson H if its mass is in the range 200–600 GeV; there are especially large enhancements in the ZZZ channel. For an annual integrated luminosity of 10 fb^{-1} at optimal incident energies about a thousand events would be produced per annum in each of the WWZ and $WW\gamma$ channels, plus about ten ZZZ events in the absence of Higgs-boson enhancements. Of order 20% of the WWZ and ZZZ final states and 30% of the $WW\gamma$ final states are in principle fully reconstructible. We present dynamical distributions with and without H effects.

I. INTRODUCTION

There is great interest in the production of two-[1,2] and three-[3–5] gauge-boson final states at future high-energy colliders, since they will allow crucial tests of the electroweak gauge theory. The predicted $WW\gamma$ and WWZ couplings will be probed by measurements of $e^+e^-\to W^+W^-$ at CERN LEP II, of $ep\to eWX$ at DESY HERA, and $pp\to V_1V_2X$ ($V=W$ or Z) at the CERN Large Hadron Collider (LHC) or the Superconducting Super Collider (SSC) (Refs. 6–9). Because of intimate cancellations between the contributions of gauge-boson exchanges in the s channel and fermion exchanges in the t and u channels, small deviations from the standard gauge-theory couplings would be amplified and would give anomalous magnitude and energy dependence to the cross sections. Amplitude zeros in radiative subprocesses such as $u\bar{d}\to W^+\gamma$ are important features of gauge theory;[10] they arise from cancellations between different exchange contributions that would be upset by the presence of anomalous interactions[6] that occur in composite models.

Attention has mainly focused on the production of two gauge bosons. In this paper we address the distributions of three gauge bosons in e^+e^- collisions, where future machines with high energies and luminosities may make experimental studies quite feasible. Such studies would be interesting because (i) triple gauge-boson production offers further independent tests of the standard theoretical framework, (ii) quartic $WWZZ$ and $WWZ\gamma$ couplings enter significantly for the first time, (iii) the standard neutral Higgs boson H plays an important role in the WWZ and ZZZ channels if its mass is in the range 200–600 GeV, and (iv) triple gauge-boson production may be a background to possible future signals from physics beyond the standard model. Cross sections for triple gauge-boson production in e^+e^- collisions have already been presented by two of us[4] using helicity-amplitude techniques; subsequently similar results have been obtained[5] with spinor-inner-product techniques. Some studies of the channel $e^+e^-\to WW\gamma$ have also been published,[11] with emphasis on situations where γ is not observed and the process is a background to Higgs-boson production in $e^+e^-\to e^+e^-W^+W^-$ or $\nu\bar{\nu}W^+W^-$. In this work we concentrate attention on final states where all three gauge bosons are observed.

Our calculations are performed using the helicity-amplitude techniques of Ref. 12. In Sec. II we explain the notation and give helicity amplitude formulas for $e^+e^-\to V_1V_2$ and $e^+e^-\to V_1V_2V_3$ processes, where the V_i are gauge vector bosons. In Sec. III we present integrated cross sections versus energy for both two- and three-gauge-boson production. Transverse-momentum and pseudorapidity cuts $p_{\gamma T}>20$ GeV and $|\eta_\gamma|<2$ are imposed on all final photons, which are expected to be seen as high-p_T electromagnetic jets. In the $e^+e^-\to WWZ$ and ZZZ channels, we show the effects of a Higgs boson on the integrated cross sections and on the diboson invariant-mass distributions, for c.m. energies $\sqrt{s}=0.5$, 1.0, 2.0 TeV. We also illustrate dynamical distributions in the WWZ and $WW\gamma$ channels versus the boson energies, transverse momenta, rapidities, polar angles, and pair opening angles.

In Sec. IV we discuss the W and Z decay branching fractions into identifiable final states, the probabilities of overlap between hadronic decay jets from different gauge bosons, and the resulting effects on the final identifiable event rates. We conclude that for c.m. energy $\sqrt{s}>0.35$ GeV and annual integrated luminosity of order 10 fb^{-1}, a substantial number of identifiable, fully reconstructible events would be produced per year in both the $e^+e^-\to WWZ$ and $e^+e^-\to WW\gamma$ channels.

II. HELICITY AMPLITUDES

A. Formalism

It has been realized that helicity amplitudes provide a convenient means for Feynman-diagram evaluations.

These amplitude-level techniques are particularly convenient for calculations involving many Feynman diagrams, where the usual trace techniques for the amplitude squared become unwieldy. Our calculations use the helicity techniques developed in Ref. 12, which we briefly summarize below.

A tree-level amplitude in e^+e^- collisions can be expressed in terms of fermion strings of the form

$$\bar{v}(p_2,\sigma_2)P_{-\tau}\not{a}_1\not{a}_2\cdots\not{a}_n u(p_1,\sigma_1)\ , \tag{1}$$

where p and σ label the initial $e^\pm$ four-momenta and helicities ($\sigma=\pm1$), $\not{a}_i=a_i^\mu\gamma_\mu$, and $P_\tau=\frac{1}{2}(1+\tau\gamma_5)$ is a chirality projection operator ($\tau=\pm1$). The a_i^μ may be formed from particle four-momenta, gauge-boson polarization vectors or fermion strings with an uncontracted Lorentz index associated with final-state fermions.

In the chiral representation the γ matrices are expressed in terms of 2×2 Pauli matrices σ and the unit matrix $\mathbf{1}$ as

$$\gamma^\mu=\begin{bmatrix}0 & \sigma_+^\mu\\ \sigma_-^\mu & 0\end{bmatrix},\quad \gamma^5=\begin{bmatrix}-1 & 0\\ 0 & 1\end{bmatrix},$$
$$\sigma_\pm^\mu=(\mathbf{1},\pm\boldsymbol{\sigma})\ , \tag{2}$$

giving

$$\not{a}=\begin{bmatrix}0 & (\not{a})_+\\ (\not{a})_- & 0\end{bmatrix},\quad (\not{a})_\pm=a_\mu\sigma_\pm^\mu\ . \tag{3}$$

The spinors are expressed in terms of two-component Weyl spinors as

$$u=\begin{bmatrix}(u)_-\\ (u)_+\end{bmatrix},\quad v=((v)_+^\dagger,(v)_-^\dagger)\ . \tag{4}$$

The Weyl spinors are given in terms of helicity eigenstates $\chi_\lambda(p)$ with $\lambda=\pm1$ by

$$u(p,\lambda)_\pm=(E\pm\lambda|\mathbf{p}|)^{1/2}\chi_\lambda(p)\ ,$$
$$v(p,\lambda)_\pm=\pm\lambda(E\mp\lambda|\mathbf{p}|)^{1/2}\chi_{-\lambda}(p)\ , \tag{5}$$

where

$$\chi_+(p)=[2|\mathbf{p}|(|\mathbf{p}|+p_z)]^{-1/2}\begin{bmatrix}|\mathbf{p}|+p_z\\ p_x+ip_y\end{bmatrix}, \tag{6}$$

$$\chi_-(p)=[2|\mathbf{p}|(|\mathbf{p}|+p_z)]^{-1/2}\begin{bmatrix}-p_x+ip_y\\ |\mathbf{p}|+p_z\end{bmatrix}. \tag{7}$$

For $p_z=-|\mathbf{p}|$ we follow the convention

$$\chi_+=\begin{bmatrix}0\\1\end{bmatrix},\quad \chi_-=\begin{bmatrix}-1\\0\end{bmatrix}. \tag{8}$$

The fermion strings can be replaced by strings of two-component spinors and 2×2 matrices. For example,

$$\begin{aligned}\bar{v}_2P_{-\tau}\not{a}_1\not{a}_2\cdots\not{a}_n u_1&=(v_2)_\tau^\dagger[a_1,a_2,\ldots,a_n]_\tau(u_1)_{\delta_n\tau}\\ &=K\chi_{-\sigma_2}^\dagger(p_2)[a_1,a_2,\ldots,a_n]_\tau\chi_{\sigma_1}(p_1)\ ,\end{aligned} \tag{9}$$

where the square brackets with subscript τ are defined by

$$\begin{aligned}&[a_1,a_2,\ldots,a_n]_\tau=(\not{a}_1)_\tau(\not{a}_2)_{-\tau}\cdots(\not{a}_n)_{\delta_n\tau}\ ,\\ &\delta_n=(-1)^{n+1}\end{aligned} \tag{10}$$

and the overall factor is

$$\begin{aligned}K=&\tau\sigma_2(E_2-\tau\sigma_2|\mathbf{p}_2|)^{1/2}\\ &\times[E_1+(-1)^{n+1}\tau\sigma_1|\mathbf{p}_1|]^{1/2}\ .\end{aligned} \tag{11}$$

The gauge-boson polarization vectors $\epsilon(Q,\alpha)$ are expressed in terms of the boson four-momenta as

$$\begin{aligned}&\epsilon^\mu(Q,\alpha=1)=(|\mathbf{Q}|Q_T)^{-1}(0,Q_xQ_z,Q_yQ_z,-Q_T^2)\ ,\\ &\epsilon^\mu(Q,\alpha=2)=Q_T^{-1}(0,-Q_y,Q_z,0)\ ,\\ &\epsilon^\mu(Q,\alpha=3)=[E_V/(M_V|\mathbf{Q}|)](|\mathbf{Q}|^2/E_V,Q_x,Q_y,Q_z)\ ,\end{aligned} \tag{12}$$

with $Q_T=(Q_x^2+Q_y^2)^{1/2}$, $E_V=(|\mathbf{Q}|^2+M_V^2)^{1/2}$. At this state it is straightforward to evaluate the helicity amplitudes numerically and to integrate over the phase space. In the results presented below we take the positive z axis to lie along the e^- beam direction.

B. $e^+e^-\to VV$ amplitudes

For the process

$$e^-(p_1,\sigma_1)+e^+(p_2,\sigma_2)\to W^-(Q_1,\alpha_1)+W^+(Q_2,\alpha_2) \tag{13}$$

there are three contributing Feynman diagrams from neutrino, Z, and γ exchanges, which give the amplitude

$$\mathcal{M}=ig^2\bar{v}(p_2,\sigma_2)\mathcal{O}u(p_1,\sigma_1)\ , \tag{14}$$

where

$$\begin{aligned}\mathcal{O}=&-(2l_1^2)^{-1}P_+\not{\epsilon}_2\not{l}_1\not{\epsilon}_1\\ &+\sum_\tau(g_\tau^eD_Z+D_\gamma x_WQ_e)P_\tau\Gamma(2,1)\ .\end{aligned} \tag{15}$$

Here

$$\begin{aligned}&l_1=p_1-Q_1,\quad D_a=(p_a^2-M_a^2+iM_a\Gamma_a)^{-1}\ ,\\ &Q_e=-1,\quad g_\tau^e=g_V^e-\tau g_A^3,\quad g_V=\tfrac{1}{2}T_3-x_WQ\ ,\\ &g_A=-\tfrac{1}{2}T_3,\quad g^2=8M_W^2G_F/\sqrt{2},\quad x_W=\sin^2\theta_W\ .\end{aligned} \tag{16}$$

The triple-gauge-boson coupling coefficient is

$$\begin{aligned}\Gamma(2,1)^\delta=&[(Q_1-Q_2)^\delta g^{\mu\nu}+(2Q_2+Q_1)^\mu g^{\delta\nu}\\ &-(2Q_1+Q_2)^\nu g^{\delta\mu}]\epsilon_{2\nu}\epsilon_{1\mu}\ .\end{aligned} \tag{17}$$

The corresponding helicity amplitudes are

$$\begin{aligned}\mathcal{M}=&ig^2(4E_1E_2)^{1/2}\chi_{-\sigma_2}^\dagger(p_2)\\ &\times\{(2l_1^2)^{-1}\delta_{1,\sigma_2}\delta_{-1,\sigma_1}[\epsilon_2l_1\epsilon_1]_{-1}\\ &-\delta_{\sigma_1,-\sigma_2}(D_Zg_{\sigma_2}^e+D_\gamma x_WQ_e)[\Gamma(2,1)]_{\sigma_1}\}\\ &\times\chi_{\sigma_1}(p_1)\ ,\end{aligned} \tag{18}$$

where $\delta_{a,b}$ is the Kronecker δ symbol.

For the process $e^+e^-\to ZZ$ there are two electron-exchange diagrams which lead to the helicity amplitudes

$$\mathcal{M}=ig_Z^2(4E_1E_2)^{1/2}(l_i^2)^{-1}\delta_{\sigma_1,-\sigma_2}(g^e_{\sigma_2})^2\chi^\dagger_{-\sigma_2}(p_2)\times[\epsilon_j l_i\epsilon_i]_{\sigma_1}\chi_{\sigma_1}(p_1) \tag{19}$$

with an implied summation over $i,j=1,2$ with $j\neq i$; $l_i=p_1-Q_i$, $g_Z=g/\cos\theta_W$.

For the process $e^+e^-\to Z\gamma$ there are again two electron-exchange diagrams which give the helicity amplitudes

$$\mathcal{M}=ig^2\frac{Q_e\sin\theta_W}{\cos\theta_W}(4E_1E_2)^{1/2}(l_i^2)^{-1}\delta_{\sigma_1,-\sigma_2}g^e_{\sigma_2}\times\chi^\dagger_{-\sigma_2}(p_2)[\epsilon_j l_i\epsilon_i]_{\sigma_1}\chi_{\sigma_1}(p_1)\ . \tag{20}$$

C. $e^+e^-\to VVV$ amplitudes

As shown in Fig. 1 there are 20 Feynman diagrams contributing to the process

$$e^-(p_1,\sigma_1)+e^+(p_2,\sigma_2)\to Z(Q_1,\alpha_1)+W^-(Q_2,\alpha_2)+W^+(Q_3,\alpha_3) \tag{21}$$

in an arbitrary gauge. In the following, we present the corresponding helicity amplitudes in the chiral representation. For economy of notation we shall write the helicity amplitudes for VVV production in the form

$$\mathcal{M}(\sigma_1,\sigma_2;\alpha_1,\alpha_2,\alpha_3)=i(4E_1E_2)^{1/2}\chi^\dagger_{-\sigma_2}(p_2)\times\mathcal{R}(\sigma_1,\sigma_2;\alpha_1,\alpha_2,\alpha_3)\chi_{\sigma_1}(p_1) \tag{22}$$

and give the reduced amplitude $\mathcal{R}$.

The three diagrams with double fermion exchanges in Fig. 1(a) contribute helicity amplitudes

$$\mathcal{R}^{(a)}=g^2g_Z\tfrac{1}{2}\delta_{1,\sigma_2}\delta_{-1,\sigma_1}\times\left[\frac{g^e_+}{l_1^2h_3^2}[\epsilon_3h_3\epsilon_2l_1\epsilon_1]_{\sigma_1}+\frac{g^\nu_+}{l_2^2h_3^2}[\epsilon_3h_3\epsilon_1l_2\epsilon_2]_{\sigma_1}+\frac{g^e_+}{l_2^2h_1^2}[\epsilon_1h_1\epsilon_3l_2\epsilon_2]_{\sigma_1}\right], \tag{23}$$

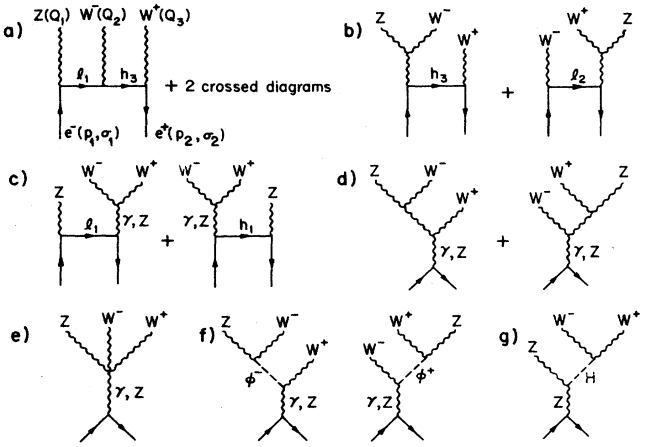

FIG. 1. Feynman diagrams for the process $e^+e^-\to W^+W^-Z$.

where $l_i=p_1-Q_i$ and $h_i=Q_i-p_2$.

The graphs in Fig. 1(b) with one neutrino and one W exchange give

$$\mathcal{R}^{(b)}=-g^3\delta_{1,\sigma_2}\delta_{-1,\sigma_1}\tfrac{1}{2}\cos\theta_W\times\left[\frac{[\Gamma^W(1,3)l_2\epsilon_2]_{\sigma_1}}{l_2^2}+\frac{[\epsilon_3h_3\Gamma^W(2,1)]_{\sigma_1}}{h_3^2}\right] \tag{24}$$

with

$$\Gamma^V(i,j)^\delta=\frac{[g^{\delta\delta'}+(1-\xi)Q_{ij}^\delta Q_{ij}^{\delta'}/(\xi Q_{ij}^2-M_V^2)]\Gamma(i,j)_{\delta'}}{Q_{ij}^2-M_V^2}\ , \tag{25}$$

where $Q_{ij}=Q_i+Q_j$. Here $\Gamma(i,j)_\delta$ is defined in Eq. (17) and ξ is the gauge parameter of the V propagator; $\xi=0$ for the unitary gauge, $\xi=1$ for the Feynman gauge, and $\xi\to\infty$ for the Landau gauge. For the photon we choose $\xi=1$ so that $\Gamma^\gamma(i,j)^\delta=\Gamma(i,j)^\delta/Q_{ij}^2$.

The graphs in Fig. 1 (c) with one electron and one Z or γ exchange give

$$\mathcal{R}^{(c)}=-g^2g_Z\delta_{\sigma_1,-\sigma_2}\left[(g^e_{\sigma_2})^2\left[\frac{[\Gamma^Z(3,2)l_1\epsilon_1]_{\sigma_1}}{l_1^2}+\frac{[\epsilon_1h_1\Gamma^Z(3,2)]_{\sigma_1}}{h_1^2}\right]+x_WQ_eg^e_{\sigma_2}\left[\frac{[\Gamma^\gamma(3,2)l_1\epsilon_1]_{\sigma_1}}{l_1^2}+\frac{[\epsilon_1h_1\Gamma^\gamma(3,2)]_{\sigma_1}}{h_1^2}\right]\right]. \tag{26}$$

The graphs in Fig. 1(d) with one W and one Z or γ exchange give

$$\mathcal{R}^{(d)}=g^3\cos\theta_W\delta_{\sigma_1,-\sigma_2}\left[g^e_{\sigma_2}\left[\frac{[\Gamma^Z(3,21)]_{\sigma_1}}{Q_{12}^2-M_W^2}+\frac{[\Gamma^Z(13,2)]_{\sigma_1}}{Q_{13}^2-M_W^2}\right]+x_WQ_e\left[\frac{[\Gamma^\gamma(3,21)]_{\sigma_1}}{Q_{12}^2-M_W^2}+\frac{[\Gamma^\gamma(13,2)]_{\sigma_1}}{Q_{13}^2-M_W^2}\right]\right], \tag{27}$$

where $\Gamma^V(i,jk)^\delta$ is defined by Eqs. (17) and (25), except that $\epsilon_{2\nu}$ in Eq. (17) should be replaced by $\Gamma(j,k)_\nu$.

The graphs of Fig. 1(e) with one γ or Z exchange and a quartic vertex give

$$\mathcal{R}^{(e)}=-g^3\cos\theta_W\delta_{\sigma_1,-\sigma_2}\{g^e_{\sigma_2}D_Z[\tilde{\Gamma}^Z(1,2,3)]_{\sigma_1} +x_W Q_e D_\gamma[\tilde{\Gamma}^\gamma(1,2,3)]_{\sigma_1}\}\ , \tag{28}$$

where

$$\tilde{\Gamma}^V(i,j,k)^\delta=[g^{\delta\delta'}+(1-\xi)P^\delta P^{\delta'}/(\xi P^2-M_V^2)]\tilde{\Gamma}(1,2,3)_{\delta'} \tag{29}$$

with

$$\tilde{\Gamma}(i,j,k)^\delta=(2g^{\delta\mu}g^{\nu\lambda}-g^{\delta\nu}g^{\mu\lambda}-g^{\delta\lambda}g^{\mu\nu}) \times\epsilon_\mu(Q_1)\epsilon_\nu(Q_2)\epsilon_\lambda(Q_3)\ , \tag{30}$$

and $P=p_1+p_2$ is the total energy momentum.

The graphs of Fig. 1(f) involving the exchange of an unphysical Higgs boson give

$$\mathcal{R}^{(f)}=-g^3\delta_{\sigma_1,-\sigma_2}M_Z^2x_W^2\left[\frac{g^e_{\sigma_2}D_Z}{\cos\theta_W}-Q_eD_\gamma\cos\theta_W\right] \times\left[\frac{[\epsilon_3]_{\sigma_1}}{Q_{12}^2-M_W^2/\xi}\epsilon_1\cdot\epsilon_2+\frac{[\epsilon_2]_{\sigma_1}}{Q_{13}^2-M_W^2/\xi}\epsilon_1\cdot\epsilon_3\right]\ . \tag{31}$$

These graphs vanish as $\xi\to0$ (i.e., in the unitary gauge).

The graph of Fig. 1(g) involving the exchange of the physical Higgs boson H gives

$$\mathcal{R}^{(g)}=-g^2g_Z\delta_{\sigma_1,-\sigma_2}g^e_{\sigma_2}M_W^2\epsilon_2\cdot\epsilon_3[\epsilon_1]_{\sigma_1}D_ZD_H\ . \tag{32}$$

For the analogous process,

$$e^-(p_1,\sigma_1)+e^+(p_2,\sigma_2)\to\gamma(Q_1,\alpha_1)+W^-(Q_2,\alpha_2) +W^+(Q_3,\alpha_3)\ , \tag{33}$$

there are 18 Feynman diagrams. They are similar to those of Fig. 1, except that the diagram of Fig. 1(a) with Z coupled to ν and the real-Higgs-boson diagram 1(g) have no counterparts here. The matrix elements $\mathcal{M}^{(a)}\cdots\mathcal{M}^{(f)}$ for $WW\gamma$ production can be recovered form those for WWZ production above by the following rules.

(i) For $\mathcal{M}^{(a)}$, multiply by $Q_e\sin\theta_W\cos\theta_W/g^e_+$ and set $g^\nu_+=0$.

(ii) For $\mathcal{M}^{(c)}$, multiply by $Q_e\sin\theta_W\cos\theta_W/g^e_{\sigma_2}$.

(iii) For $\mathcal{M}^{(b)}$, $\mathcal{M}^{(d)}$, $\mathcal{M}^{(e)}$, multiply by $\sin\theta_W/\cos\theta_W$.

(iv) For $\mathcal{M}^{(f)}$, multiply by $-\cos\theta_W/\sin\theta_W$.

Using the helicity amplitude method, it is straightforward to incorporate the subsequent decays of the vector bosons. To obtain the complete helicity amplitude with fermions as the final states, the polarization vectors of outgoing vector bosons are replaced by the appropriate fermion currents to which the vector bosons couple:

$$\epsilon^*_\mu(p)\to-c(V)D_V\sum_\tau c^f_\tau\bar{u}(f)P_\tau\gamma_\mu v(\bar{f})\ , \tag{34}$$

where

$$c(V)=\begin{cases}eQ_f & \text{for } V=\gamma\ ,\\ V_{ff'}g/\sqrt{2} & \text{for } V=W\ ,\\ g/\cos\theta_W & \text{for } V=Z\ ,\end{cases} \qquad c^f_\tau=\begin{cases}1 & \text{for } V=\gamma\ ,\\ \delta_{1\tau} & \text{for } V=W\ ,\\ g^f_V-\tau g^f_A & \text{for } V=Z\ .\end{cases} \tag{35}$$

Here $V_{ff'}$ is a fermion mixing matrix element and D_V is defined in Eq. (16).

The helicity amplitudes for $e^+e^-\to ZZZ$ are given in Ref. 4 and will not be repeated here.

III. CROSS SECTIONS AND GAUGE-BOSON DISTRIBUTIONS

We are interested in final states where all three gauge bosons are identified and measured. We assume that W and Z will be identified by their hadronic and charged-lepton decays (Sec. IV below) and a final photon will be identified as an electromagnetic jet of neutral origin; accordingly transverse-momentum and pseudorapidity cuts

$$p_{\gamma T}>20\text{ GeV},\quad |\eta_\gamma|<2 \tag{36}$$

have been imposed on all final photons [$\eta=\ln\cot(\frac{1}{2}\theta)$].

Figure 2 shows the integrated cross sections versus c.m. energy for two- and three-gauge-boson final states produced in e^+e^- collisions. In this figure, possible enhancements from a physical Higgs boson H have been

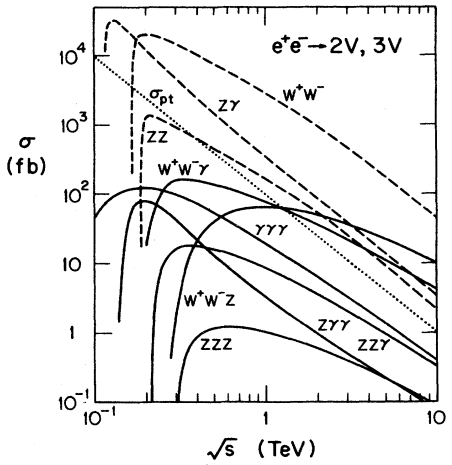

FIG. 2. Integrated cross sections for the production of two and three gauge bosons in e^+e^- collisions, vs c.m. energy $\sqrt{s}$, omitting Higgs-boson effects. The QED point cross section σ_{pt} is shown for comparison.

TABLE I. Values of $R=\sigma(VVV)/\sigma_{pt}$ and corresponding annual event rates for $e^+e^-\to WWZ$, ZZZ, and $WW\gamma$ assuming a luminosity 10 fb^{-1} per year.

$\sqrt{s}$ (TeV)	$R(W^+W^-Z)$	$N(W^+W^-Z)$	$R(ZZZ)$	$N(ZZZ)$	$R(W^+W^-\gamma)$	$N(W^+W^-\gamma)$
	$m_H<2M_W$ or $m_H\gtrsim 1$ TeV (negligible Higgs-boson contribution)					
0.35	1.5×10^{-2}	1.2×10^{2}	7.1×10^{-4}	6	0.20	1.6×10^{3}
0.5	9.7×10^{-2}	3.9×10^{2}	2.9×10^{-3}	12	0.35	1.4×10^{3}
1.0	5.8×10^{-1}	5.8×10^{2}	1.0×10^{-2}	10	0.73	7.3×10^{2}
2.0	1.8	4.4×10^{2}	2.4×10^{-2}	6	1.4	3.4×10^{2}
			$m_H=0.2$ TeV			
0.35	2.9×10^{-2}	2.4×10^{2}	9.5×10^{-3}	77		
0.5	1.2×10^{-1}	4.6×10^{2}	1.5×10^{-2}	58		
1.0	0.6	6.0×10^{2}	2.3×10^{-2}	22		
2.0	1.8	4.5×10^{2}	3.2×10^{-2}	8		

omitted and the lowest-order QED "point" cross section $\sigma_{pt}=\sigma(e^+e^-\to\gamma^*\to\mu^+\mu^-)=4\pi\alpha^2/(3s)$ has been introduced as a convenient comparison scale. The two-gauge-boson cross sections are from 1 to 2 orders of magnitude above those for three gauge bosons, depending on $\sqrt{s}$. Nevertheless, the triple-gauge-boson cross sections approach 100 fb so that for an e^+e^- collider with an annual integrated luminosity of 10 fb^{-1} the total event rates for the WWZ and $WW\gamma$ channels would be about one thousand per year; see Table I.

A standard-model neutral Higgs boson H will enhance the cross sections for W^+W^-Z and ZZZ as shown in Fig. 3. The production of H in e^+e^- collisions comes from its coupling to the Z boson line in Fig. 1(g). The enhancement in the $3V$ process is appreciable only when $2M_V<m_H<\sqrt{s}-M_V$ and is largest when m_H is of order $2M_V$. The presence of H gives peaks in the distributions versus diboson invariant masses M_{WW} and M_{ZZ} that are illustrated in Fig. 4 for $\sqrt{s}=0.5$, 1.0, 2.0 TeV with a range of m_H values.

Bosons from $H\to V_1V_2$ decay are dominantly longitudinally polarized in the H rest frame.[13] This gives rise to $V_1\to ab$ decay angular distributions of the form $d\sigma/d\cos\theta^*\sim\sin^2\theta^*$, where θ^* is the polar angle in the V_1 rest frame defined with respect to the V_2 momentum vector. Transverse polarization, on the other hand, gives

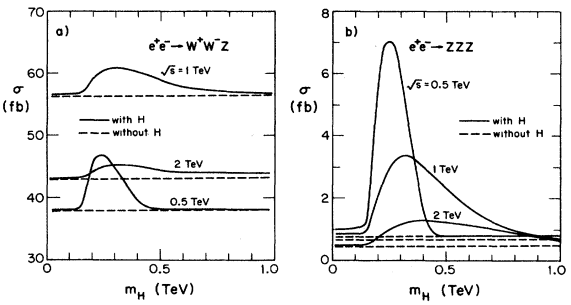

FIG. 3. Integrated cross sections for (a) $e^+e^-\to WWZ$ and (b) $e^+e^-\to ZZZ$ vs Higgs-boson mass showing the enhancement from the possible presence of a heavy standard-model Higgs boson, for $\sqrt{s}=0.5$, 1.0, 2.0 TeV.

$d\sigma/d\cos\theta^*\sim(1+\cos^2\theta^*)$ distributions (averaging the two decay products a and b). Polarization therefore offers another way to confirm the Higgs-boson signal, if the non-Higgs-boson contributions are mainly transverse. In $e^+e^-\to W^+W^-Z$ events, for example, the $\cos\theta^*$ distribution in the decay of W^+ or W^- in each bin of invariant mass M_{WW} is determined by the fraction of events P_L^W with longitudinal polarization: namely,

$$\sigma^{-1}d\sigma/d\cos\theta^*=\tfrac{3}{8}[1+P_L+(1-3P_L)\cos^2\theta^*]\ . \quad (37)$$

In a mass bin corresponding to a strong H signal, P_L approaches 1 and the distribution approaches a $\sin^2\theta^*$ shape. Calculations show that the non-Higgs-boson contributions are indeed mainly transverse. Figure 5(a) illustrates the $\cos\theta^*$ dependence of W^- decays in $e^+e^-\to W^+W^-Z$ for $\sqrt{s}=0.5$, $m_H=0.2$ TeV; summing over all events we have $P_L^W\simeq0.3$ and a concave-upward shape, but in the bin $180<M_{WW}<220$ GeV we have $P_L^W\simeq0.5$ and a markedly convex shape. Figure 5(b) shows the corresponding dependence of P_L^W on M_{WW}; it is clear that P_L^W would be even more enhanced if it were practicable to select a narrower bin at the Higgs-boson peak. If we increase m_H above 0.2 TeV the longitudinal-polarization fraction P_L of the Higgs-boson signal will increase toward 1.0, since $\Gamma(H\to W_LW_L)\sim m_H^3/M_W^2$ whereas $\Gamma(H\to W_TW_T)\sim M_W^2/m_H$.

Figure 6 shows the transverse-momentum distributions of W and Z in the WWZ channel at $\sqrt{s}=0.5$, 1.0, 2.0, TeV with $m_H=0.2$ or 0.4 TeV; the W^+ and W^- curves coincide. The Jacobian peak in $p_T(Z)$ at the value

$$p_T(Z,\text{peak})=[s^2-2s(M_Z^2+m_H^2)+(m_H^2-M_Z^2)^2]^{1/2}/(2\sqrt{s}\,) \quad (38)$$

is due to the two-body kinematics of the Higgs-boson contribution in Fig. 1(g). Figure 7 shows the W and Z c.m. energy distributions for the same choices of energy and Higgs-boson mass. The spike in E_Z at the value

$$E_Z(\text{peak})=(s+M_Z^2-m_H^2)/(2\sqrt{s}\,) \quad (39)$$

is again due to the two-body kinematics of the Higgs-boson contribution (smeared by the widths of H and Z);

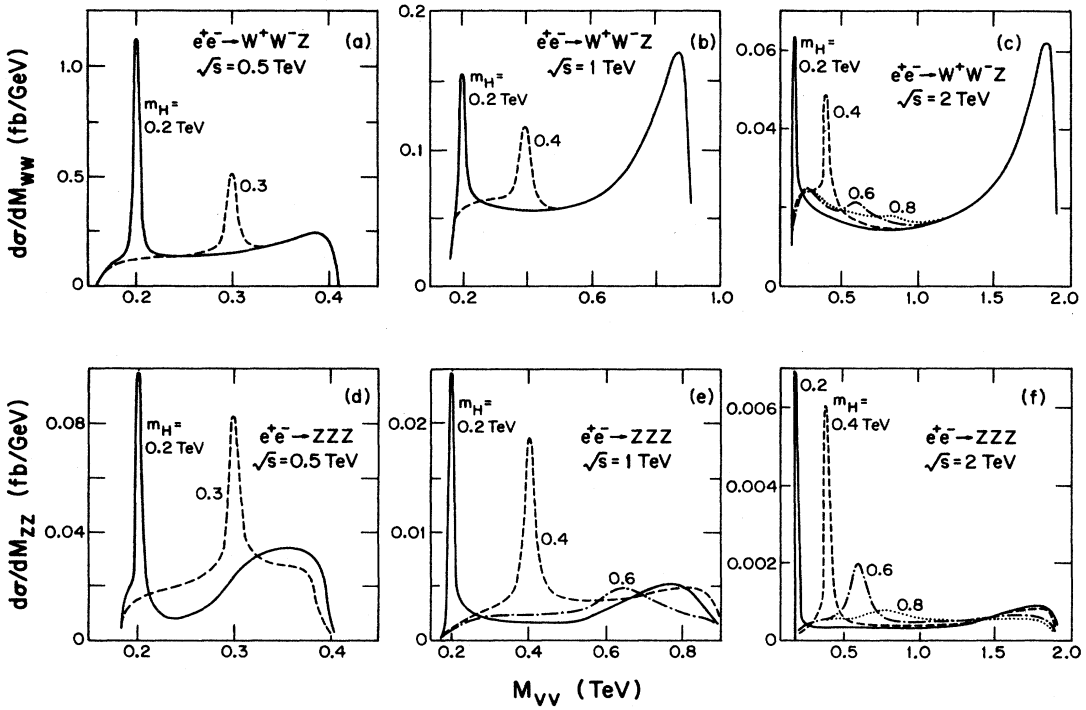

FIG. 4. Effects of Higgs-boson contribution on diboson invariant-mass distributions. The M_{WW} distribution in $e^+e^- \to WWZ$ is shown for (a) $\sqrt{s}=0.5$ TeV, (b) $\sqrt{s}=1.0$ TeV, and (c) $\sqrt{s}=2.0$ TeV. The M_{ZZ} distribution in $e^+e^- \to ZZZ$ is shown for (d) $\sqrt{s}=0.5$ TeV, (e) $\sqrt{s}=1.0$ TeV, (f) $\sqrt{s}=2.0$ TeV, averaged over the three ZZ pairings.

it is hard to distinguish in the case of Fig. 7(c).

Figure 8 shows the distributions versus W^+, W^-, and Z c.m. rapidities in the WWZ channel, defining the z axis to lie along the e^- beam direction. The three curves peak in different regions and the peaks broaden systematically as energy increases. There are no distinctive Higgs-boson effects here and the case of no Higgs-boson contribution is shown. Figure 9 illustrates the dependence on gauge-boson polar angles θ_V and diboson opening angles $\theta_{VV'}$ in the WWZ c.m. frame. The spike in θ_{WW} comes from the Higgs-boson contribution; its position is determined by m_H and its width is related to the H width.

Similar distributions for $e^+e^- \to WW\gamma$ events are shown in Figs. 10 and 11. Here there is no Higgs effect, but otherwise the features broadly resemble those of the WWZ case.

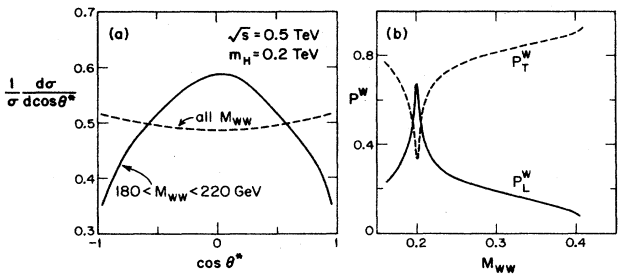

FIG. 5. (a) Dependence of $e^+e^- \to W^+W^-Z$ cross section on $\cos\theta^*$ of W^- decay at $\sqrt{s}=0.5$, $m_H=0.2$ TeV; W^+ results are the same; the dashed curve refers to all events, the solid curve refers to the mass bin $0.18 < M_{WW} < 0.22$ TeV. (b) Corresponding dependence of the longitudinal and transverse polarization fractions P_L^W and P_T^W on WW invariant mass, denoted by solid and dashed curves, respectively.

IV. BRANCHING FRACTIONS AND EVENT RATES

The identification of three gauge-boson events depends on the channels into which the $W^\pm$ and Z decay. For the branching fractions of the individual W and Z bosons we assume $m_t=45$ GeV with three neutrino species and use the calculated values

$$\begin{aligned} Z &\to q\bar{q}, \ 0.70 , \\ & e\bar{e}, \ 0.03 , \\ & \mu\bar{\mu}, \ 0.03 , \\ & \tau\bar{\tau}, \ 0.03 , \\ & \nu\bar{\nu}, \ 0.20 ; \\ W &\to q\bar{q}', \ 0.73 , \\ & e\nu, \ 0.09 , \\ & \mu\nu, \ 0.09 , \\ & \tau\nu, \ 0.09 . \end{aligned} \tag{40}$$

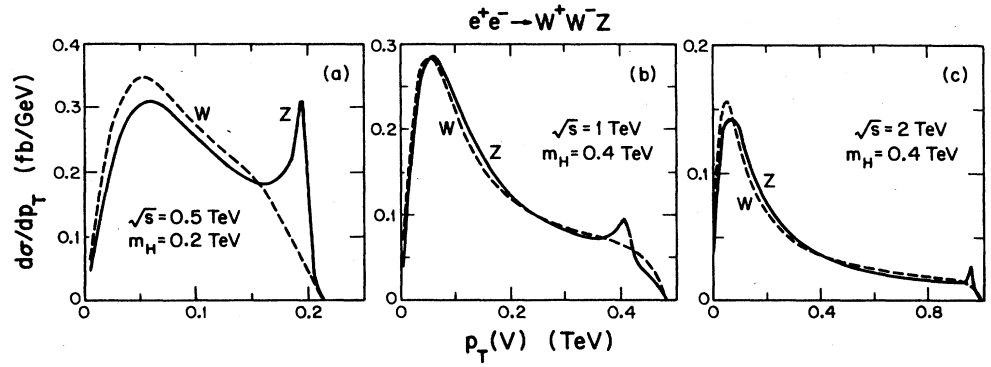

FIG. 6. W and Z momentum distributions transverse to the beam axis in the WWZ channel for (a) $\sqrt{s}=0.5$, $m_H=0.2$ TeV, (b) $\sqrt{s}=1.0$, $m_H=0.4$ TeV, and (c) $\sqrt{s}=2.0$, $m_H=0.4$ TeV.

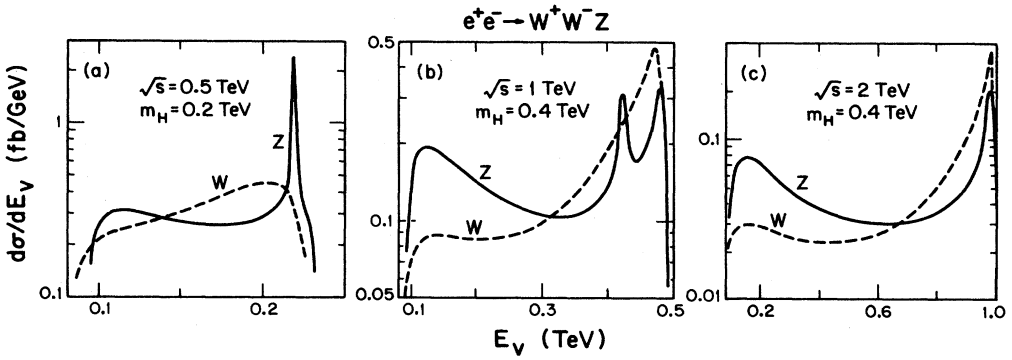

FIG. 7. W and Z c.m. energy distributions in the WWZ channel for (a) $\sqrt{s}=0.5$, $m_H=0.2$ TeV, (b) $\sqrt{s}=1.0$, $m_H=0.4$ TeV, and (c) $\sqrt{s}=2.0$, $m_H=0.4$ TeV.

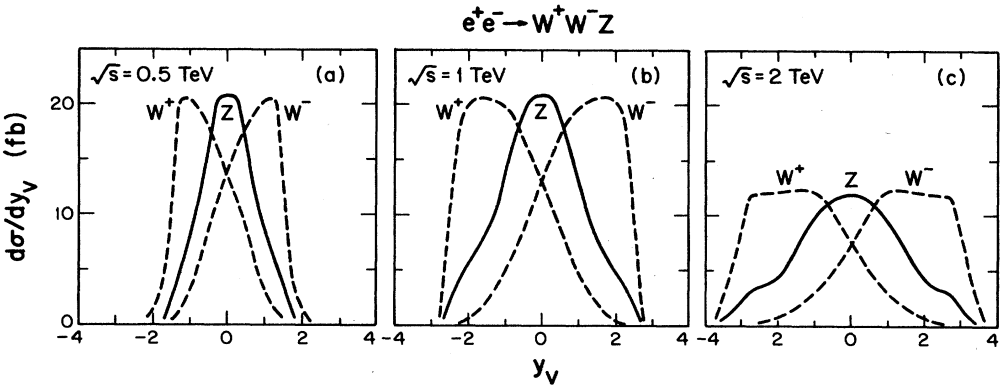

FIG. 8. W^+, W^-, and Z c.m. rapidity distributions in the WWZ channel for (a) $\sqrt{s}=0.5$ TeV, (b) $\sqrt{s}=1.0$ TeV, and (c) $\sqrt{s}=2.0$ TeV. There is no distinctive Higgs effect here and we show the case of no Higgs-boson contribution.

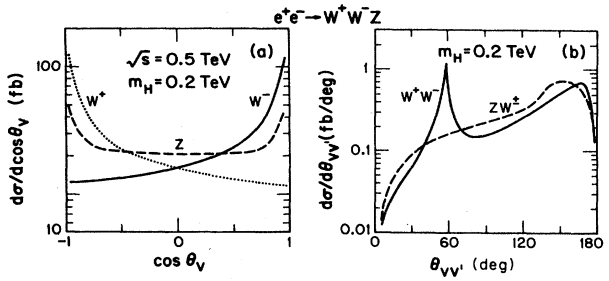

FIG. 9. Distributions in the WWZ channel vs (a) gauge-boson polar angles θ_V and (b) diboson opening angles $\theta_{VV'}$ in the c.m. frame, for $\sqrt{s}=0.5$, $m_H=0.2$ TeV.

Here, the $q\bar{q}$ and $q\bar{q}'$ final states are summed over all contributing quark flavors and lead primarily to two-jet states. For a two-jet or two-lepton state to be identified, its invariant mass must reconstruct the mass of the parent Z or W. This can be achieved in principle for e^+e^-, $\mu^+\mu^-$, and pairs of purely hadronic jets. However, in decays to heavy-quark jets (initiated by c, b, or t) there are appreciable probabilities of semileptonic decays with unmeasurable neutrinos; the latter will only be identified when the neutrinos are soft and subtract little from the visible invariant mass (or when vertex detectors identify the weakly decaying heavy flavors). Including semileptonic modes where the visible invariant mass

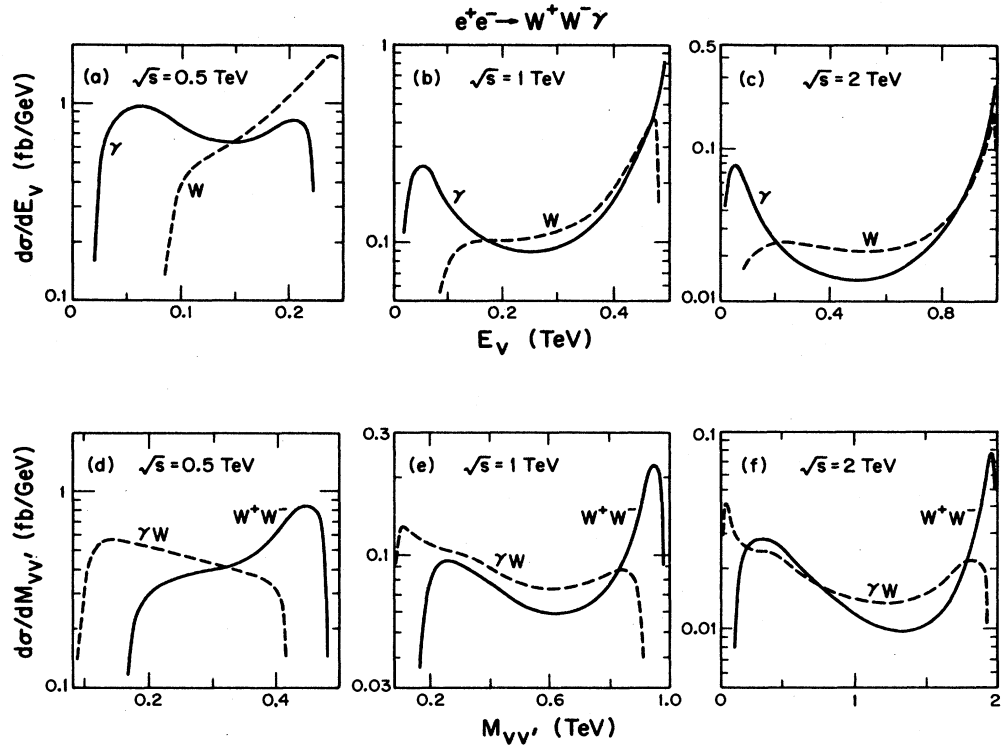

FIG. 10. Calculation results in the $e^+e^- \to WW\gamma$ channel: distributions vs gauge-boson c.m. energies E_V at (a) $\sqrt{s}=0.5$ TeV, (b) $\sqrt{s}=1.0$ TeV, (c) $\sqrt{s}=2.0$ TeV (W^+ and W^- curves coincide); distributions vs diboson invariant masses $M_{VV'}$ at (d) $\sqrt{s}=0.5$ TeV, (e) $\sqrt{s}=1.0$ TeV, and (f) $\sqrt{s}=2.0$ TeV ($W^+\gamma$ and $W^-\gamma$ curves coincide).

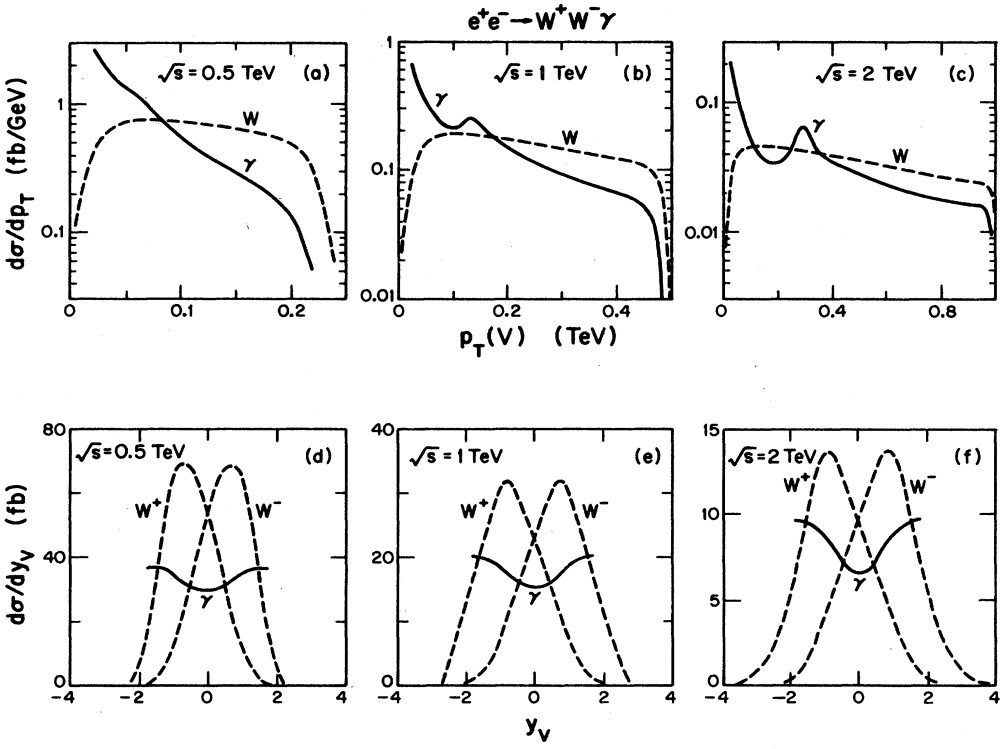

FIG. 11. Distributions in the WW_γ channel vs gauge-boson transverse momenta $p_T(V)$ at (a) $\sqrt{s}=0.5$ TeV, (b) $\sqrt{s}=1.0$ TeV, and (c) $\sqrt{s}=2.0$ TeV; distribution vs gauge-boson rapidities y_V at (d) $\sqrt{s}=0.5$ TeV, (e) $\sqrt{s}=1.0$ TeV, and (f) $\sqrt{s}=2.0$ TeV.

exceeds 95% of the parent W or Z mass, the *reconstructible* branching fractions are

$$\begin{aligned} Z\to q\bar{q},&\quad 0.60\ ,\\ e\bar{e},&\quad 0.03\ ,\\ \mu\bar{\mu},&\quad 0.03\ ;\\ W\to q\bar{q}',&\quad 0.61\ . \end{aligned} \tag{41}$$

In practice these values will be reduced a little by detector resolution and by cutting the tails of the Z and W resonance mass distributions, but we take them as the basis for the present discussion. A final-state photon can be identified as an electromagnetic shower with a neutral initiator (i.e., no charged track in a central detector), with high efficiency in principle.

Ideally, with a highly hermetic detector, one could measure the total missing energy and missing three-momentum for the events that occur at $\sqrt{s}=2E_{\rm beam}$. Then those modes where just one of the W or Z decayed into neutrinos could also be reconstructed. Because of the strong beamstrahlung effects[14] expected at future e^+e^- high-energy linear colliders, many events will actually occur at lower energies; it is likely that such measurements will be restricted here to the missing transverse momentum $\not{p}_T$. Nevertheless, it should still be possible to reconstruct a substantial fraction of the $W\to l\nu$ ($l=e$ or μ) decays where the transverse mass[15]

$$m_T(l\not{p}_T)=[(|\mathbf{p}_{lT}|+|\not{\mathbf{p}}_T|)^2-(\not{\mathbf{p}}_{lT}+\not{\mathbf{p}}_T)^2]^{1/2} \tag{42}$$

lies close to M_W while the other two gauge bosons appear as hadronic jets. The fraction of events reconstructible in this way will depend on the experimental $\not{p}_T$ resolution. We therefore regard Eq. (41) as providing only a conservative lower bound on the eventually reconstructible decays.

Another factor affecting the identification of VVV events is jet overlap. If two jets from two different gauge bosons overlap substantially, it will not be possible to separate them and reconstruct the masses accurately. Also if an electron from $Z\to e^+e^-$ or $W\to e\nu$ decay overlaps with a jet, it may well escape identification and confuse the kinematics. To study this question we have calculated the cross-section dependence on a cut Δ_0, requiring all opening angles $\Delta\theta$ between pairs of leptons or jets (from two different gauge-boson parents) to exceed Δ_0:

$$\begin{aligned} \Delta_{\rm min}\equiv\min\Delta\theta(&\text{jet}+\text{jet or lepton}\\ &+\text{jet from different } V)\ge\Delta_0\ . \end{aligned} \tag{43}$$

Figure 12 shows the distributions versus $\Delta_{\rm min}$ for $e^+e^-\to WWZ$ and $WW\gamma$, for typical energies $\sqrt{s}=0.5$, 1.0, and 2.0 TeV.

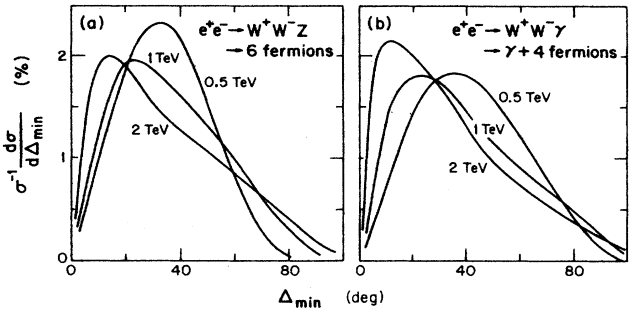

FIG. 12. Dependence on the minimum opening angle $\Delta_{\rm min}$ of Eq. (43) for (a) $e^+e^-\to WWZ$ and (b) $e^+e^-\to WW\gamma$.

Yet another factor is the beam pipe. There is inevitably a loss of information about final particles emerging near the beam axis, so for practical purposes we require all final leptons and jets to lie outside the extreme forward and backward cone defined by an angle θ_0:

$$\theta_0\le\theta(\text{lepton or jet})\le\pi-\theta_0\ . \tag{44}$$

Note that our photon cuts Eq. (36) already include a minimum angle requirement with $\theta_0=15.4°$ on the photon direction.

The Δ_0 and θ_0 cuts are approximately independent. If realistically we require both $\Delta_0=15°$ and $\theta_0=10°$ simultaneously, the fractions of events satisfying these cuts will be

$\sqrt{s}$ (TeV)	WWZ	$WW\gamma$
0.5	0.84	0.88
1.0	0.70	0.75
2.0	0.53	0.63

(45)

Putting together the results of Eqs. (41) and (45), and remembering the possibility of identifying some other decays in addition, we conclude that at least 20% of $e^+e^-\to W^+W^-Z$ and 32% of $e^+e^-\to W^+W^-\gamma$ events should be fully reconstructible at $\sqrt{s}=0.5$ TeV (falling to 13% and 23%, respectively, at $\sqrt{s}=2.0$ TeV).

Since the product of branching fraction and geometrical efficiency for reconstructible final states is substantial, the crucial factor for event rates will be the production cross section. We summarize in Table I the numbers of WWZ, ZZZ, and $WW\gamma$ events that would be produced at e^+e^- colliders of various c.m. energies for an estimated[16] integrated annual luminosity of 10 fb^{-1}=10^{40} cm^{-2}. The optimal energy for $WW\gamma$ production is about $\sqrt{s}=0.35$ TeV; the optimal energy for WWZ production is 1 TeV. For detection efficiencies of order 20–30%, hundreds of events would be obtained per year with this luminosity to test the standard-model gauge couplings.

Reconstructible events in the WWZ and $WW\gamma$ channels should be essentially free of backgrounds, due to the

simultaneous mass-shell constraints. Continuum processes such as $e^+e^- \to W^+W^-$, $t\bar{t}$, $q\bar{q}gg$, etc., may have integrated cross sections that are an order of magnitude or more larger than the $3V$ signals, but the requirement that three gauge bosons be simultaneously reconstructed will strongly suppress such backgrounds (presuming reasonable detector resolution).

ACKNOWLEDGMENTS

This research was supported in part by the University of Wisconsin Research Committee with funds granted by the Wisconsin Alumni Research Foundation and in part by the U.S. Department of Energy under Contract No. DE-AC02-76ER00881.

[1]R. W. Brown and K. O. Mikaelian, Phys. Rev. D **19**, 922 (1979); R. W. Brown, D. Sahdev, and K. O. Mikaelian, *ibid.* **20**, 1164 (1979).

[2]E. Eichten, I. Hinchliffe, K. Lane, and C. Quigg, Rev. Mod. Phys. **56**, 579 (1984); **58**, 1065(E) (1986).

[3]M. S. Chanowitz and M. K. Gaillard, Phys. Lett. **142B**, 85 (1984); M. Golden and S. Sharpe, Nucl. Phys. **B261**, 217 (1985).

[4]V. Barger and T. Han, Phys. Lett. B **212**, 117 (1988).

[5]A. Tofighi-Niaki and J. F. Gunion, Phys. Rev. D (to be published).

[6]K. Hagiwara, R. D. Peccei, D. Zeppenfeld, and K. Hikasa, Nucl. Phys. **B282**, 253 (1987); D. Zeppenfeld and S. Willenbrock, Phys. Rev. D **37**, 1775 (1988); U. Baur and D. Zeppenfeld, Nucl. Phys. **B308**, 127 (1988).

[7]E. Grabrielli, Mod. Phys. Lett. **A1**, 465 (1986).

[8]D. A. Dicus, S. L. Wilson, and R. Vega, Phys. Lett. B **192**, 231 (1987); D. A. Dicus and R. Vega, Phys. Rev. D **37**, 2474 (1988).

[9]A. Abbasabadi and W. W. Repko, Phys. Rev. D **37**, 2668 (1988).

[10]K. O. Mikaelian, M. A. Samuel, and D. Sahdev, Phys. Rev. Lett. **43**, 746 (1979); C. J. Goebel, F. Halzen, and J. P. Leveille, Phys. Rev. D **23**, 2682 (1981); S. J. Brodsky and R. W. Brown, Phys. Rev. Lett. **49**, 966 (1982); R. W. Brown, K. L. Kowalski, and S. J. Brodsky, Phys. Rev. D **28**, 624 (1983); J. Cortés, K. Hagiwara, and F. Herzog, Nucl. Phys. **B278**, 26 (1986); M. A. Samuel and J. H. Reid, Prog. Theor. Phys. **76**, 184 (1986).

[11]M. Greco, G. Pancheri, and A. Grau, Phys. Lett. B **205**, 573 (1988).

[12]K. Hagiwara and D. Zeppenfeld, Nucl. Phys. **B274**, 1 (1986).

[13]M. J. Duncan, G. L. Kane, and W. W. Repko, Nucl. Phys. **B272**, 517 (1986); M. J. Duncan, Phys. Lett. B **179**, 393 (1986); C. L. Bilchak, R. W. Brown, and J. D. Stroughair, Phys. Rev. D **29**, 375 (1984).

[14]For a discussion of the implications for experiments at future e^+e^- colliders, see G. J. Feldman, Report No. SLAC-PUB-4564, 1988 (unpublished); C. Ahn *et al.*, SLAC Report No. 329, 1988 (unpublished); D. L. Burke, Snowmass conference report, 1988 (unpublished).

[15]UA1 Collaboration, Phys. Lett. **122B**, 103 (1983); V. Barger, A. D. Martin, and R. J. N. Phillips, Z. Phys. C **21**, 99 (1983); J. Smith, W. L. Van Neerven, and J. A. M. Vermaseren, Phys. Rev. Lett. **50**, 1738 (1983).

[16]P. Grosse-Wiesmann, Report No. SLAC-PUB-4545, 1988 (unpublished); J. H. Mulvey, in *Proceedings of the Workshop on Physics at Future Accelerators,* La Thiule, Italy, 1987, edited by J. H. Mulvey (CERN Report No. 87-07, Geneva, Switzerland, 1987).